Manuscript title:

Differentiation of focal nodular hyperplasia and hepatocellular adenoma using qualitative and quantitative imaging features and classification and regression tree analysis

Short title:

CART for differentiation of FNH and HCA

Authors:

Talal M Alamri, MD [1,2]

Milena Cerny, MD [1,3]

Mohammad Al Shaikh, MD [1,4]

Jean-Sébastien Billiard, MD [1]

Damien Olivié, MD[1]

Miguel Chagnon, MSc, P.Stat. [5]

An Tang, MD, MSc [1, 3] https://orcid.org/0000-0001-8967-5503

Affiliations:

[1] Department of Radiology, Centre hospitalier de l'Université de Montréal (CHUM), Montréal, Qc, Canada.

[2] Department of Radiology, King Saud Medical City, Riyad, Saudi Arabia.

[3] Centre de recherche du Centre hospitalier de l'Université de Montréal (CRCHUM), Montréal, Qc, Canada.

[4] Department of Radiology, King Fahad Medical City, Riyad, Saudi Arabia.

[5] Department of Mathematics and Statistics, Université de Montréal, Montréal, QC, Canada.

Corresponding author:

An Tang, MD, MSc, FRCPC

Full Professor of Radiology

Department of Radiology

Centre hospitalier de l'Université de Montréal

1058 rue Saint-Denis, Montréal, Québec, Canada, H2X 3J4.

Telephone: (514) 944-4213

Fax: (514) 412-7359

E-mail: an.tang@umontreal.ca

Manuscript title:

Differentiation of focal nodular hyperplasia and hepatocellular adenoma using qualitative and quantitative imaging features and classification and regression tree analysis

Abbreviations:

CART	classification and regression tree
CE	contrast enhanced
CER	contrast enhancement ratio
FNH	focal nodular hyperplasia
HBP	hepatobiliary phase
HCA	hepatocellular adenoma
LLC	lesion-to-liver contrast
NPV	negative predictive value
PPV	positive predictive value
ROI	region of interest
RSER	relative signal enhancement ratio
SI	signal intensity
SIR	signal intensity ratio

ABSTRACT

Purpose: To assess qualitative and quantitative analysis of gadoxetate disodium-enhanced hepatobiliary phase MR imaging (MRI) and assess the performance of classification and regression tree analysis for the differentiation of focal nodular hyperplasia (FNH) and hepatocellular adenoma (HCA).

Materials and Methods: This retrospective study was approved by our local ethics committee. One hundred seventy patients suspected of having FNH or HCA underwent gadoxetate disodium-enhanced MRI. The reference standard was either pathology or follow-up imaging. Two readers reviewed images to identify qualitative imaging features and measure signal intensity on unenhanced, dynamic, and hepatobiliary phase images. For quantitative analysis, contrast enhancement ratio (CER), lesion-to-liver contrast (LLC), signal intensity ratio (SIR), and relative signal enhancement ratio (RSER) were calculated. A classification and regression tree (CART) analysis was developed.

Results: Eighty-five patients met the inclusion criteria, with a total of 97 FNHs and 43 HCAs. For qualitative analysis, the T1 signal intensity on the hepatobiliary phase provided the highest overall classification performance (91.9% sensitivity, 90.1% specificity, and 90.9% accuracy). For quantitative analysis, RSER in the hepatobiliary phase with a threshold of 0.723 provided the highest classification performance (92.6% sensitivity and 89.4% specificity) to differentiate FNHs from HCAs. A CART model based on five qualitative imaging features provided an accuracy of 94.4% (95% confidence interval: 90.0% - 98.9%).

Conclusion: Gadoxetate disodium-enhanced hepatobiliary phase provides high diagnostic performance as demonstrated in quantitative and qualitative analysis in differentiation of FNH and HCA, supported by a CART decision model.

INTRODUCTION

Focal nodular hyperplasia (FNH) and hepatocellular adenoma (HCA) are two common focal liver lesions occurring in women of childbearing age. Their prevalence in the general adult population is estimated to be between 0.4-3.0% and 0.007-0.012% respectively (1-3).

Magnetic resonance (MR) imaging is commonly used to differentiate these two types of lesions, as certain imaging features favor one or the other. However, several imaging features are not pathognomonic and can be found in both lesions. Hepatobiliary contrast agents have increased the diagnostic performance of MRI for differentiation of FNH and HCA (4, 5). In particular, a gadoxetate disodium-enhanced hepatobiliary phase may play an important role in differentiating these two lesions (6). Although both types of tumor are generally considered benign, their natural history differs. FNHs are often found incidentally and their long-term evolution includes stability and regression, which justifies conservative management for this “no-touch lesion” (7). In contrast, HCAs have a risk of complications such as rupture, hemorrhage (8), and malignant transformation in 4,2% of cases (9), they may require image-guided therapy or surgical resection.

Considering the differences in clinical risk, an accurate diagnosis is required. Qualitative imaging features, including some assessable with a hepatobiliary contrast agent, contribute to MRI-based classification of FNH and HCA (4, 5). In addition, quantitative imaging features based on contrast enhancement ratios may provide objective criteria for lesion classification (10). A systematic review by Mclnnes et al reported good diagnostic accuracy of the

hepatobiliary phase for the diagnosis of FNH versus HCA; however the authors noted that there were relatively few studies, with heterogeneous results and at high risk for bias (6). Hence, there is a need to assess qualitative and quantitative imaging features and to identify clinically helpful imaging features.

The purpose of this study was to assess qualitative and quantitative imaging features of gadoxetate disodium-enhanced hepatobiliary phase MR imaging (MRI) for differentiation of FNH versus HCA. A secondary objective was to develop a diagnostic algorithm based on qualitative imaging features to differentiate these two types of lesions.

MATERIALS AND METHODS

Study Design and Subjects

This retrospective, cross-sectional, single-site study was approved by the *Centre hospitalier de l'Université de Montréal* Institutional Review Board. Patient consent for data analysis was waived.

The eligibility period for our study was between August 2010 and March 2015. Patients with gadoxetate disodium-enhanced MR imaging for suspected FNH or HCA, and presence of at least one diagnosis reference standard (histopathology or imaging follow-up) per patient were included. Inadequate examination or incomplete follow-up were excluded**.** Clinical, imaging, and histopathological data were retrieved from picture archiving and communication system (PACS) and electronic medical records, and documented in a database and assigned to a consecutive study number.

MRI Examination

Liver examinations were performed at 1.5 T (Torso coil; GE Medical Systems, Milwaukee, WI; 8-channel coil) or 3.0 T (dStream Torso coil; Achieva TX, Philips Healthcare, Best, The Netherlands; 32-channel coil). The patients were examined in the supine position, and the receiver coil was positioned to cover the upper abdomen. All MR images were acquired by using parallel imaging sensitivity encoding with a reduction factor of two. The protocol is detailed in **Table 1** and included contrast-enhanced sequences acquired in breath-hold axial T1-weighted fat-saturated three-dimensional precontrast and dynamic contrast-enhanced

(arterial, 20 seconds; portal venous, 70 seconds; transitional, 2-5 min), axial and coronal hepatobiliary phase (20min), with gradient-recalled echo sequence (shortest TR; shortest TE; 10°; abdomen; 5 mm; 0 mm). We used the contrast agent gadoxetate disodium (Primovist; Bayer Schering, Berlin, Germany) with a dose administrated according to patient weight (0.025mmol/kg), through antecubital at a rate of 1mL/sec followed by a 15 mL saline flush.

Imaging Analysis

All MR images were randomly reviewed on PACS workstations (Impax version 6.6, Agfa HealthCare, Mortsel, Belgium), by two abdominal radiologists ([initials withheld to preserve blinding], respectively 22 and 24 years of experience) who reviewed the entire examinations. The readers were blinded to the clinical information and histologic findings.

Qualitative analysis.— We assessed the presence of morphological features (central scar, capsule, blood products, fat content, atoll sign (11), and lobulations); the predominant signal characteristic of lesions on T2-weighted and T1-weighted images, diffusion-weighted images (DWI) at b-value = 800 s/mm^2 and on apparent diffusion coefficient (ADC) map; the enhancement of each lesion relative to that of the surrounding liver parenchyma on gadoxetate disodium-enhanced sequences (arterial, portal venous, transitional phase, and hepatobiliary phase); and the enhancement pattern on the hepatobiliary phase (homogenous, heterogenous, presence of hyperintense rim, hypointense core, or hyperintense core).

Quantitative analysis.— We assessed the number and size of lesions (number of tumor per patient, initial and final diameter of each lesion and calculated growth during the follow-up

period). We measured the SI on all T1-weighted images (unenhanced and after gadoxetate disodium-enhanced sequences) of each lesion, adjacent liver parenchyma and paravertebral muscle. The ROIs were placed by an abdominal radiology fellow (M.C, 3 years). ROIs on paravertebral muscles were used for normalization. Contrast enhancement ratio (CER) was calculated as follow: [((SI $lesion_{CE}$ – SI $liver_{UE}$)/SI $lesion_{CE}$) x 100] where CE is the SI of the lesion on gadoxetate disodium-enhanced images and UE is the SI of the lesion on unenhanced images. Lesion-to-liver contrast (LLC) was calculated as follow: [(SI $lesion_{CE}$- SI $liver_{CE}$)/SI $muscle_{CE}$]. Signal intensity ratio (SIR) was calculated as follow: [(SI $lesion_{CE}$/ SI $liver_{CE}$)] for each sequence. Relative signal enhancement ratio (RSER) was calculated as follow: [(SI $lesion_{CE}$/SI $lesion_{UE}$) / (SI $liver_{CE}$/SI $liver_{UE}$)], which corresponds to the rate of enhancement and de-enhancement of lesion to liver parenchyma through time (12).

Diagnosis Standard of Reference

Reference standard for diagnosis was either histopathological analysis or follow-up MR imaging.

Statistical Analysis

The agreement between readers for each feature was assessed with kappa (κ) statistics and observed agreement. The values of κ were expressed using Landis & Koch classification as follows: 0–0.20, slight agreement; 0.21–0.40, fair; 0.41–0.60, moderate; 0.61–0.80, substantial; 0.81–1, almost perfect agreement (13). *P*-value for qualitative features was calculated using chi-squared test adjusted for patient cluster effect. For values of quantitative features, *P*-value was based on generalized estimating equation (GEE), done with SAS version 9.4. Diagnostic

performance of qualitative features determined using a classification and regression tree, and for quantitative features, an optimum cut-off point set based Youden's index.

Decision Tree Model

For development of decision tree, R package for classification and regression tree (CART) (14) "rpart" was applied, using R software version 3.3.3 and package rpart version 4.1.12. The tree is built step by step. At the first step, the variable that best divides (according to the Gini criterion) the observation into two groups is identified. The data is separated according to the resulting classification rule. This process is then applied, at each subsequent step, to the subgroups obtained previously. The process ends for a sub-group when its size is less than a fixed criterion (i.e., $n = 5$ in this case) or when no improvement can be made.

RESULTS

Study Population

A total of 85 patients, with 97 FNHs and 43 HCAs met the inclusion criteria (**Fig 1**). The FNH group included 62 patients (5 males, 57 females) with a mean age of 39 (± 12.2), and total of 97 lesions. The median diameter of FNHs was 29.5 mm (8-129 mm). The reference standard was histopathology in 17 (17.5%) and follow-up imaging in 80 (82.5%). The HCA group included 23 patients (1 male, 22 females) with a mean age of 37.6 (± 6.9), and total of 43 lesions. The median diameter of HCAs was 27.5 mm (10 – 115 mm). The reference standard was histopathology in 14 (32.6%) and follow-up imaging in 29 (67.4%) lesions. Characteristics of patients and lesions are summarized in **Table 2**. Representative MR imaging examples of FNA and HCA are shown in **Fig 2** and **3**, respectively.

Agreement between radiologists

Table 3 summarizes inter-reader agreement for qualitative imaging. Inter-reader agreement was highest with substantial agreement for the presence of fat content and central scar (κ = 0.65 and 0.65 and proportion of observed agreement = 0.93 and 0.85, respectively); followed by appearance on transitional phase with substantial agreement (κ = 0.61 and proportion of observed agreement = 0.76); appearance on portal and hepatobiliary phase with moderate agreement (κ = 0.60 and 0.60 and proportion of observed agreement = 0.78 and 0.76 respectively).

Qualitative Analysis

Table 4 summarizes qualitative MR imaging characteristics. Our analysis demonstrates significant differences in all morphological features between FNH and HCA lesions ($P < 0.05$) with the exception of atoll sign. FNHs had a central scar in 44 (45.4%), fat content in 4 (4.1%), and lobulations in 48 (49.5%) of cases. No FNHs had a capsule or blood products. HCAs had fat content in 10 (23.3%) of cases.

For signal characteristics, except for T1-weighted signal ($P < 0.022$), no significant differences in signal characteristics were observed on T2-weighted, diffusion-weighted imaging and apparent diffusion coefficient. Enhancement characteristics of FNH lesions were significantly different from that of HCAs during all dynamic phases ($P < .0001$) except for the arterial phase. FNHs were hyperintense in the portal phase in 76 (78.4%), hyperintense in the transitional phase in 68 (70.1%), and hyperintense in the hepatobiliary phase in 66 (68.0%) of cases. FNHs were homogeneous in 44 (45.4%) and heterogeneous in 32 (32%) in the hepatobiliary phase. HCAs were more likely to demonstrate partial washout on portal phase in 5 (11.6%), hypointense signal on transitional phase in 32 (74.4%) and hypointense signal on hepatobiliary phase in 39 (92.9%) of cases.

Quantitative Analysis

Table 5 summarizes quantitative MR imaging characteristics. No significant differences were found in the number, size, or growth. Several enhancement ratios in various vascular phases significantly differed between FNH and HCA. CERs were significantly different in all vascular phases ($P < .0001$). The difference in CER between the two groups was largest in hepatobiliary

phase, with mean values of 215.3 for FNH and 56.4 for HCA. LLCs were significantly different in all vascular phases ($P < .002$). The difference in LLC between the two groups was largest in hepatobiliary phase, with mean values of 0.1 for FNH and -1.13 for HCA. SIRs were significantly different in arterial and hepatobiliary phases ($P < .0001$). The difference in SIR between the two groups was largest in hepatobiliary phase, with mean values of 1.07 for FNH and 0.67 for HCA. RSERs were significantly different in portal, transitional, and hepatobiliary phases ($P < .03$). The difference in RSERs between the two groups was largest in hepatobiliary phase, with mean values for of 1.19 for FNH and 0.33 for HCA.

Diagnostic Performance

Table 6 summarizes the diagnostic performance of qualitative and quantitative analyses that were significant at univariate analysis. Among qualitative features, the sensitivity was highest for the enhancement in the hepatobiliary phase (91.9%), the specificity in the portal venous phase (99.0%), and the accuracy in the hepatobiliary phase (90.1%). Among quantitative features, the sensitivity was highest for the RSER in the hepatobiliary phase (92.6%), the specificity was highest for RSER in the transitional and hepatobiliary phases (both 89.4%), and the accuracy was highest for the RSER in hepatobiliary phase (90.2%).

Classification and Regression Tree

Figure 5 provides a CART model based exclusively on qualitative imaging features so that it can be easily used clinically for decision support without requiring calculation. Based on data, our CART model included five imaging characteristics organized hierarchically.

We studied a total of 9 qualitative characteristics from a total of 15 characteristics that were statistically significant which may be related to outcome. In the implementation of CART, the dataset is split into the two subgroups that are most different with the intention to reach a homogenous subgroup. The first partitioning predictor in the decision model tree was based on the signal intensity on the hepatobiliary phase which could be either hyper- or iso-intense vs. hypointense. The second partitioning predictor was the appearance in the transitional phase which could be either hyper-, iso-, or hypointense vs. partially hypointense. The third partitioning predictor was the presence of fat content which could be no vs. yes. The fourth partitioning predictor was the hepatobiliary phase pattern which could be heterogeneous or with hyperintense rim vs. homogeneous or with hypointense core. The fifth partioning predictor was appearance on portal phase which could be hyperintense or isointense. The model based on five qualitative imaging features provided an accuracy of 94.4% (95% confidence interval: 90.0% - 98.9%).

DISCUSSION

The purpose of this study was to assess the diagnostic performance of qualitative and quantitative imaging features for differentiation of FNH versus HCA and to develop a diagnostic algorithm to prioritize qualitative imaging features. In this single-center retrospective study, patients with gadoxetate disodium-enhanced MR imaging for suspected FNH or HCA were included.

Inter-reader agreement was substantial for fat content, central scar, and appearance on transitional phase and moderate for appearance on portal and hepatobiliary phases. Interestingly, inter-reader agreement was lowest for blood products, atoll sign, and capsule. Ngu et al (15) have previously assessed inter-observer agreement for a variety of liver lesions on the hepatobiliary phase of gadoxetate disodium-enhanced MR imaging and found substantial to almost perfect agreement. They also noted that inter-observer agreement may improve with radiologists' experience. Ronot et al have previously assessed the inter-reader agreement for MRI classification of HCA subtypes (16). Their study reported almost perfect agreement ($\kappa = 0.86$) for classification of HCA subtypes with gadoterate meglumine-enhanced MRI; however, the study did not include FNHs in their cohort. To our knowledge, no prior studies have assessed the inter-reader agreement of gadoxetate disodium-enhanced MR imaging features in a cohort composed exclusively of FNHs and HCAs.

For qualitative analysis, there were significant differences between FNH and HCA lesions in our cohort for most morphological features (except for the atoll sign), T1-weighted signal

characteristics and enhancement characteristics during all dynamic phases (except for the arterial phase). FNHs are more likely to have a central scar, lobulations, T1-weighted hypo or isointensity, portal phase hyperintensity, transitional phase hyperintensity, and hepatobiliary phase iso- or hyperintensity. In contrast, HCAs are more likely to have a capsule, fat content, portal phase hypointensity, transitional phase hypointensity and hepatobiliary phase hypointensity. In our cohort, 90.7% of FNHs were either iso- or hyperintense in the hepatobiliary phase compared to 7.1% of HCAs. This is in agreement with prior studies reporting that central scars and lobulations were more likely to be present in FNHs and fat content in HCAs (5, 17, 18). Our results are also in line with prior studies, including a systematic review by McInnes et al, that have reported high diagnostic accuracy for the differentiation of FNHs from HCAs on gadoxetate disodium-enhanced hepatobiliary phases (4, 6, 17). A systemic review and meta-analysis by Suh et al (19) showed that FNHs were iso- or hyperintense in arterial phase, portal phase and hepatobiliary phases in 99%, 97% and 93%, respectively. Signal intensity on the hepatobiliary phase was considered highly accurate for differentiating FNHs from HCAs. This finding has been attributed to gadoxetate disodium uptake by the organic anion transporting polypeptide 8 (OATP 8) transporter which is abundant in FNHs and minimal or absent in HCA (20, 21). Van Kessel et al (22) described a correlation between appearance of FNHs in hepatobiliary phase and the number and type of bile ducts, extent of fibrosis, presence of inflammation and extent of vascular proliferation.

For quantitative analysis based on enhancement ratios, CER, LLC, SIR and RSER provided significant differences between FNHs and HCAs in several vascular phases. Among these the various vascular phases, the differences in enhancement ratios were typically largest in the

hepatobiliary phase. In our cohort, RSER in the hepatobiliary phase with a threshold of 0.723 provided the highest classification performance (92.6% sensitivity and 89.4% specificity) to differentiate FNHs from HCAs. Our results are in agreement with the few studies that have previously assessed quantitative analyses. Grazioli et al (4) found significant differences in CER and LLC between FNHs and HCAs that were increasingly widening from the arterial to the portal venous, transitional and hepatobiliary phases with gadoxetate disodium. Haimerl et al (29) found that FNHs demonstrated higher CER in comparison to HCAs, hepatocellular carcinomas, metastases and hemangioma. They also found that FNH had higher LLC than HCAs in the hepatobiliary phase.

While calculation of enhancement ratios in several vascular phases is feasible in a research setting, there is a need for simple decision criteria based on imaging features to differentiate FNHs from HCAs in daily clinical practice. Hence, we proposed a decision tree model based on a machine learning technique known as CART (14). This clinical algorithm provides a stepwise approach for differentiation of the two types of lesions based on qualitative features assessed by radiologists. Although six potential morphological features and four signal characteristics were considered in this CART analysis, only five of those qualitative features were used as nodes in the tree. All these five features were significantly different between FNHs and HCAs at univariate analysis. To our knowledge, there is no previous CART application to differentiate FNH and HCA.

There are certain limitations to our study. First, our study contains an incorporation bias because the index test contains qualitative imaging features that may have been considered

by the radiologists who read the follow-up MRI examinations serving as the reference standard. However, reliance on a composite reference standard that included histopathology or follow-up MRI may have reduced this bias. Second, we only assessed lesions that were either diagnosed as FNH and HCA, whereas an emerging trend is to differentiate genomic subtypes of HCAs. However, a clinically applicable algorithm providing practical guidance is still required for clinical differentiation of FNH and HCA. Finally, we proposed a CART model based on a training dataset. Validation in an independent cohort should be performed in a future study.

In summary, qualitative and quantitative analyses of gadoxetate disodium-enhanced hepatobiliary phase MRI both provide high diagnostic performance. We proposed a CART decision model based on five qualitative imaging features that can be used as an algorithm in applicable a clinical setting. to differentiate FNH and HCA.

Bibliography

1. Marrero JA, Ahn J, Rajender Reddy K. ACG clinical guideline: the diagnosis and management of focal liver lesions. Am J Gastroenterol 2014;109(9):1328-1347; quiz 1348. doi: 10.1038/ajg.2014.213

2. Vilgrain V, Uzan F, Brancatelli G, Federle MP, Zappa M, Menu Y. Prevalence of Hepatic Hemangioma in Patients with Focal Nodular Hyperplasia: MR Imaging Analysis. Radiology 2003;229(1):75-79. doi: 10.1148/radiol.2291021284

3. Maillette de Buy Wenniger L, Terpstra V, Beuers U. Focal Nodular Hyperplasia and Hepatic Adenoma: Epidemiology and Pathology. Digestive Surgery 2010;27(1):24-31. doi: 10.1159/000268404

4. Grazioli L, Bondioni MP, Haradome H, Motosugi U, Tinti R, Frittoli B, Gambarini S, Donato F, Colagrande S. Hepatocellular adenoma and focal nodular hyperplasia: value of gadoxetic acid-enhanced MR imaging in differential diagnosis. Radiology 2012;262(2):520-529. doi: 10.1148/radiol.11101742

5. Bieze M, van den Esschert JW, Nio CY, Verheij J, Reitsma JB, Terpstra V, van Gulik TM, Phoa SSKS. Diagnostic Accuracy of MRI in Differentiating Hepatocellular Adenoma From Focal Nodular Hyperplasia: Prospective Study of the Additional Value of Gadoxetate Disodium. American Journal of Roentgenology 2012;199(1):26-34. doi: 10.2214/ajr.11.7750

6. McInnes MD, Hibbert RM, Inácio JR, Schieda N. Focal Nodular Hyperplasia and Hepatocellular Adenoma: Accuracy of Gadoxetic Acid-enhanced MR Imaging--A Systematic Review. Radiology 2015;277(2):413-423. doi: 10.1148/radiol.2015142986

7. Kuo Y-H, Wang J-H, Lu S-N, Hung C-H, Wei Y-C, Hu T-H, Chen C-H, Yen Y-H, Lee C-M, Eng H-L. Natural course of hepatic focal nodular hyperplasia: A long-term follow-up study with sonography. Journal of Clinical Ultrasound 2009;37(3):132-137. doi: 10.1002/jcu.20533

8. Deneve JL, Pawlik TM, Cunningham S, Clary B, Reddy S, Scoggins CR, Martin RC, D'Angelica M, Staley CA, Choti MA, Jarnagin WR, Schulick RD, Kooby DA. Liver cell adenoma: a multicenter analysis of risk factors for rupture and malignancy. Ann Surg Oncol 2009;16(3):640-648. doi: 10.1245/s10434-008-0275-6

9. Farges O, Dokmak S. Malignant transformation of liver adenoma: an analysis of the literature. Dig Surg 2010;27(1):32-38. doi: 10.1159/000268405

10. Grazioli L, Bondioni MP, Haradome H, Motosugi U, Tinti R, Frittoli B, Gambarini S, Donato F, Colagrande S. Hepatocellular Adenoma and Focal Nodular Hyperplasia: Value of Gadoxetic Acid–enhanced MR Imaging in Differential Diagnosis. Radiology 2012;262(2):520-529. doi: doi:10.1148/radiol.11101742

11. Aalten SMv, Thomeer MGJ, Terkivatan T, Dwarkasing RS, Verheij J, Man RAd, IJzermans JNM. Hepatocellular Adenomas: Correlation of MR Imaging Findings with Pathologic Subtype Classification. Radiology 2011;261(1):172-181. doi: 10.1148/radiol.11110023

12. Tse JR, Naini BV, Lu DSK, Raman SS. Qualitative and Quantitative Gadoxetic Acid–enhanced MR Imaging Helps Subtype Hepatocellular Adenomas. Radiology 2016;279(1):118-127. doi: 10.1148/radiol.2015142449

13. Landis JR, Koch GG. An application of hierarchical kappa-type statistics in the assessment of majority agreement among multiple observers. Biometrics 1977;33(2):363-374.

14. Breiman L, Friedman JH, Olshen RA, Stone CJ. Classification And Regression Trees. New York, 1984.

15. Ngu S, Lebron-Zapata L, Pomeranz C, Katz S, Gerst S, Zheng J, Moskowitz C, Do RK. Inter-observer agreement on the assessment of relative liver lesion signal intensity on hepatobiliary phase imaging with gadoxetate (Gd-EOB-DTPA). Abdom Radiol (NY) 2016;41(1):50-55. doi: 10.1007/s00261-015-0609-3

16. Ronot M, Bahrami S, Calderaro J, Valla DC, Bedossa P, Belghiti J, Vilgrain V, Paradis V. Hepatocellular adenomas: accuracy of magnetic resonance imaging and liver biopsy in subtype classification. Hepatology 2011;53(4):1182-1191. doi: 10.1002/hep.24147

17. Grieser C, Steffen IG, Kramme IB, Blaker H, Kilic E, Perez Fernandez CM, Seehofer D, Schott E, Hamm B, Denecke T. Gadoxetic acid enhanced MRI for differentiation of FNH and HCA: a single centre experience. Eur Radiol 2014;24(6):1339-1348. doi: 10.1007/s00330-014-3144-7

18. Grazioli L, Federle MP, Brancatelli G, Ichikawa T, Olivetti L, Blachar A. Hepatic adenomas: imaging and pathologic findings. Radiographics 2001;21(4):877-892; discussion 892-874. doi: 10.1148/radiographics.21.4.g01jl04877

19. Suh CH, Kim KW, Kim GY, Shin YM, Kim PN, Park SH. The diagnostic value of Gd-EOB-DTPA-MRI for the diagnosis of focal nodular hyperplasia: a systematic review and meta-analysis. Eur Radiol 2015;25(4):950-960. doi: 10.1007/s00330-014-3499-9

20. Vander Borght S, Libbrecht L, Blokzijl H, Faber KN, Moshage H, Aerts R, Van Steenbergen W, Jansen PL, Desmet VJ, Roskams TA. Diagnostic and pathogenetic implications of the expression of hepatic transporters in focal lesions occurring in normal liver. J Pathol 2005;207(4):471-482. doi: 10.1002/path.1852

21. Kitao A, Zen Y, Matsui O, Gabata T, Kobayashi S, Koda W, Kozaka K, Yoneda N, Yamashita T, Kaneko S, Nakanuma Y. Hepatocellular carcinoma: signal intensity at gadoxetic acid-enhanced MR Imaging--correlation with molecular transporters and histopathologic features. Radiology 2010;256(3):817-826. doi: 10.1148/radiol.10092214
22. van Kessel CS, de Boer E, ten Kate FJ, Brosens LA, Veldhuis WB, van Leeuwen MS. Focal nodular hyperplasia: hepatobiliary enhancement patterns on gadoxetic-acid contrast-enhanced MRI. Abdom Imaging 2013;38(3):490-501. doi: 10.1007/s00261-012-9916-0
23. Reizine E, Ronot M, Pigneur F, Purcell Y, Mulé S, Dioguardi Burgio M, Calderaro J, Amaddeo G, Laurent A, Vilgrain V, Luciani A. Iso- or hyperintensity of hepatocellular adenomas on hepatobiliary phase does not always correspond to hepatospecific contrast-agent uptake: importance for tumor subtyping. Eur Radiol 2019;29(7):3791-3801. doi: 10.1007/s00330-019-06150-7
24. Ba-Ssalamah A, Antunes C, Feier D, Bastati N, Hodge JC, Stift J, Cipriano MA, Wrba F, Trauner M, Herold CJ, Caseiro-Alves F. Morphologic and Molecular Features of Hepatocellular Adenoma with Gadoxetic Acid–enhanced MR Imaging. Radiology 2015;277(1):104-113. doi: 10.1148/radiol.2015142366
25. Agarwal S, Fuentes-Orrego JM, Arnason T, Misdraji J, Jhaveri KS, Harisinghani M, Hahn PF. Inflammatory hepatocellular adenomas can mimic focal nodular hyperplasia on gadoxetic acid-enhanced MRI. AJR Am J Roentgenol 2014;203(4):W408-414. doi: 10.2214/ajr.13.12251
26. Thomeer MG, Willemssen FE, Biermann KK, El Addouli H, de Man RA, Ijzermans JN, Dwarkasing RS. MRI features of inflammatory hepatocellular adenomas on hepatocyte phase imaging with liver-specific contrast agents. J Magn Reson Imaging 2014;39(5):1259-1264. doi: 10.1002/jmri.24281

27. Reizine E, Amaddeo G, Pigneur F, Baranes L, Legou F, Mulé S, Zegai B, Roche V, Laurent A, Rahmouni A, Calderaro J, Luciani A. Quantitative correlation between uptake of Gd-BOPTA on hepatobiliary phase and tumor molecular features in patients with benign hepatocellular lesions. Eur Radiol 2018;28(10):4243-4253. doi: 10.1007/s00330-018-5438-7

28. Yoneda N, Matsui O, Kitao A, Kozaka K, Kobayashi S, Sasaki M, Yoshida K, Inoue D, Minami T, Gabata T. Benign Hepatocellular Nodules: Hepatobiliary Phase of Gadoxetic Acid–enhanced MR Imaging Based on Molecular Background. RadioGraphics 2016;36(7):2010-2027. doi: 10.1148/rg.2016160037

29. Haimerl M, Wächtler M, Zeman F, Verloh N, Platzek I, Schreyer AG, Stroszczynski C, Wiggermann P. Quantitative evaluation of enhancement patterns in focal solid liver lesions with Gd-EOB-DTPA-enhanced MRI. PLoS One 2014;9(6):e100315. doi: 10.1371/journal.pone.0100315

TABLES

Table 1. MR Imaging Technique.

Coronal breath-hold T2-weighted single-shot fast spin echo: Repetition time (TR), 2000 msec; echo time (TE), 80 msec; flip angle, 90°; field of view, abdomen; section thickness, 5 mm; 0 mm gap.
Axial respiratory-triggered T2-weighted fat-saturated fast spin echo: TR, 2500 msec; TE, 80 msec; flip angle, 90°; field of view, abdomen; section thickness, 5 mm; 0 mm gap.
Axial respiratory-triggered diffusion-weighted echo-planar imaging: Shortest TR; shortest TE; flip angle, 90°; field of view, abdomen; section thickness, 5 mm; 0 mm gap; b values, 0, 400 and 800 sec/mm^2.
Axial breath-hold T1-weighted dual-echo gradient-recalled echo: Shortest TR; shortest TE; flip angle, 10°; field of view, abdomen; section thickness, 5 mm; 0 mm gap.
Axial breath-hold T1-weighted fat-saturated three-dimensional with gradient-recalled echo sequence: Shortest TR; shortest TE; flip angle, 10°; field of view, abdomen; section thickness, 5 mm; 0 mm gap. •Unenhanced •Late arterial phase, based on automated contrast material bolus-tracking technique •Portal venous phase, 70 seconds. •Transitional phase, 2-5 minutes. •Hepatobiliary phase, 20 minutes.

Axial and coronal breath-hold T1-weighted fat-saturated three-dimensional with gradient-recalled echo sequence: shortest TR; shortest TE; flip angle, 10°; field of view, abdomen; section thickness, 5 mm; 0 mm gap during hepatobiliary phase at 20 min.

Table 2. Characteristics of Patients and Lesions.

Characteristics	Patients with FNH (*n* = 62)	Patients with HCA (*n* = 23)
Sex		
Male	5 (8.1%)	1 (4.3%)
Female	57 (91.9%)	22 (95.7%)
Age (y)		
Mean ± SD*	39.15 ±12.21	37.61 ± 6.99
Number of lesion	97	43
Number of lesion per patient		
Median (min-max)	1 (1-3)	1 (1-5)
Lesion diameter mm	29.5 (8 – 129)	27.5 (10-115)
Median (min-max)		
Diagnostic reference standard		
Histopathology	17 (17.5%)	14 (32.6%)
Follow-up imaging	80 (82.5%)	29 (67.4%)
Histologic diagnosis subcategory		
FNH	97 (100%)	0 (0%)
HCA	0 (0%)	24 (55.8%)
HCA subtype	0 (0%)	15 (34.9%)
Adenomatosis	0 (0%)	3 (7.0%)
Unclassified	0 (0%)	1 (2.3%)

Note.—Data are numbers patients of nodules, with either range or percentages in parentheses. *SD : Standard deviation.

Table 3. Inter-reader Agreement for Qualitative Features.

Category	Characteristics	Kappa [95% CI]	Observed agreement
Morphological features	Central scar	0.65 [0.49, 0.79]	0.85 [0.77, 0.91]
	Lobulations	0.40 [0.26, 0.56]	0.72 [0.65, 0.79]
	Capsule	0.17 [-0.04, 0.45]	0.94 [0.90, 0.97]
	Blood products	-0.03 [-0.07, -0.01]	0.92 [0.84, 0.97]
	Fat content	0.65 [0.37, 0.88]	0.93 [0.87, 0.98]
	Atoll sign	0.13 [-0.07, 0.38]	0.88 [0.82, 0.93]
Signal characteristics	T2-weighted signal	0.41 [0.26, 0.54]	0.73 [0.65, 0.79]
	T1-weighted signal	0.39 [0.23, 0.55]	0.63 [0.53, 0.72]
	Mass DWI signal b800	0.52 [0.31, 0.70]	0.78 [0.68, 0.86]
	Mass DWI signal ADC	0.57 [0.36, 0.73]	0.81 [0.74, 0.88]
Enhancement characteristics	Arterial phase	0.53 [0.16, 0.78]	0.94 [0.88, 0.98]
	Portal venous phase	0.60 [0.45, 0.73]	0.78 [0.70, 0.85]
	Transitional phase	0.61 [0.48, 0.72]	0.76 [0.68, 0.83]
	Hepatobiliary phase	0.60 [0.46, 0.71]	0.76 [0.68, 0.84]
	HBP enhancement pattern	0.50 [0.34, 0.61]	0.69 [0.59, 0.77]

Note.—Estimation with 95% bias-corrected confidence interval based on 1000 bootstrap sample taking account patient cluster effect. *ADC* = apparent diffusion coefficient. *CI* = confidence interval. *DWI* = diffusion weighted imaging. HBP =hepatobiliary phase.

Table 4. Qualitative MR Imaging Characteristics of Focal Nodular Hyperplasia (FNH) and Hepatocellular Adenoma (HCA).

Characteristic	FNH (*n* = 97)	HCA (*n* = 43)	*P* value
Morphological features			
Central scar			
- No	53 (54.6%)	42 (97.7%)	< 0.001
- Yes	44 (45.4%)	1 (2.3%)	
Capsule			
- No	97 (100%)	41 (95.3%)	0.032
- Yes	0 (0%)	2 (4.7%)	
Blood products			
- No	97 (100%)	43 (100%)	
- Yes	0 (0%)	0 (0%)	
Fat content			
- No	93 (95.9%)	33 (76.7%)	0.014
- Yes	4 (4.1%)	10 (23.3%)	
Atoll sign			
- No	96 (99.0%)	41 (95.3%)	0.172
- Yes	1 (1.0%)	2 (4.7%)	
Lobulations			
- No	49 (50.5%)	38 (88.4%)	< 0.001
- Yes	48 (49.5%)	5 (11.6%)	
Signal characteristics			
T2-weighted			
- Hypointense	0 (0%)	1 (2.3%)	
- Isointense	37 (38.1%)	14 (32.6%)	0.605
- Hyperintense	59 (60.8%)	28 (65.1%)	
T1-weighted			
- Hypointense	39 (40.2%)	12 (27.9%)	

- Isointense	52 (53.6%)	18 (41.9%)	0.022
- Hyperintense	6 (6.2%)	13 (30.2%)	
DWI (b = 800 s/mm^2)			
- Hypointense	1 (1.1%)	0 (0%)	
- Isointense	13 (14.4%)	6 (15.8%)	0.343
- Hyperintense	76 (84.4%)	29 (76.3%)	
- Absent*	0 (0%)	3 (7.9%)	
ADC			
- Hypointense	3 (3.4%)	3 (7.9%)	0.707
- Isointense	74 (85.1%)	32 (84.2%)	
- Hyperintense	6 (6.9%)	0 (0%)	
- Absent*	4 (4.6%)	3 (7.9%)	
Enhancement			
Arterial phase			
- Hypointense	1 (1.1%)	1 (2.3%)	
- Isointense	1 (1.1%)	6 (14.0%)	0.054
- Hyperintense	95 (97.9%)	36 (83.7%)	
Portal phase			
- Hypointense	1 (1%)	11 (25.6%)	
- Isointense	20 (20.6%)	16 (37.2%)	< 0.001
- Hyperintense	76 (78.4%)	11 (25.6%)	
- Partial washout	0 (0%)	5 (11.6%)	
Transitional phase			
- Hypointense	7 (7.2%)	32 (74.4%)	
- Isointense	16 (16.5%)	4 (9.3%)	
- Hyperintense	68 (70.1%)	5 (11.6%)	< 0.001
- Partially hypointense	6 (6.2%)	2 (4.7%)	
Hepatobiliary phase			
- Hypointense	9 (9.3%)	39 (92.9%)	
- Isointense	22 (22.7%)	0 (0%)	< 0.001

- Hyperintense	66 (68.0%)	3 (7.1%)	
- Partially hypointense	0 (0%)	1 (2.3%)	
Enhancement pattern			
Hepatobiliary phase			
- Homogeneous	44 (45.4%)	37 (86%)	
- Heterogeneous	31 (32%)	2 (4.7%)	
- w/ hyperintense rim	9 (9.3%)	0 (0%)	0.004
- w/ hypointense core	13 (13.4%)	3 (7.0%)	
- w/ hyperintense core	0 (0%)	1 (2.3%)	

Note.— *P*-value based on adjusted chi-squared test adjusted for patient cluster effect. *ADC* = apparent diffusion coefficient. *DWI* = diffusion-weighted imaging. *Missing sequences were marked as absent.

Table 5. Quantitative MR Imaging Characteristics of Focal Nodular Hyperplasia (FNH) and Hepatocellular Adenoma (HCA).

Charateristics	FNH (*n* = 97)	HCA (*n* = 43)	*P*-value
Number, size, and growth			
- Mass number	1.45 ± 0.65	1.86 ± 1.17	0.1142
- Maximum diameter initial	37.7 ± 26.5	34.2 ± 21.8	0.4421
- Maximum diameter final	36.4 ± 26.7	29 ± 16.6	0.2727
- Initial to final diameter ratio	1.07 ± 0.22	1.08 ± 0.2	0.4114
- Final to initial diameter ratio	0.96 ± 0.14	0.95 ± 0.16	0.3243
- Absolute growth per year	-0.88 ± 3.24	-0.25 ± 5.0	0.2127
- Relative growth per year	-0.02 ± 0.12	-0.01 ± 0.15	0.1805
Enhancement ratios			
- CER arterial	181.1 ± 111.7	100.6 ± 48.2	<.0001
- CER portal	185.2 ± 93.7	106.57 ± 61.2	<.0001
- CER transitional	188.3 ± 87.7	91.7 ± 68.5	<.0001
- CER hepatobiliary	215.3 ± 144.9	56.43 ± 67.8	<.0001
- LLC unenhanced	0.02 ± 0.32	0.06 ± 0.32	0.6670
- LLC arterial	0.91 ± 0.58	0.72 ± 0.56	0.0021
- LLC portal	0.32 ± 0.42	0.02 ± 0.47	0.0002
- LLC transitional	0.19 ± 0.43	-0.34 ± 0.53	<.0001
- LLC hepatobiliary	0.1 ± 0.65	-1.13 ± 0.95	<.0001
- SIR arterial	1.75 ± 0.49	1.47 ± 0.38	<.0001
- SIR hepatobiliary	1.07 ± 0.29	0.67 ± 0.22	<.0001
- RSER arterial	4.06 ± 4.93	3.31 ± 2.3	0.2193
- RSER portal	1.35 ± 0.55	1.08 ± 0.64	0.0289
- RSER transitional	1.19 ± 0.39	0.64 ± 0.53	<.0001
- RSER hepatobiliary	1.11 ± 0.51	0.33 ± 0.36	<.0001

Note.— *CER* = contrast enhacement ratio. *LLC* = liver-lesion contrast. *RSER* = relative signal enhancement ratio. *SIR* = signal intensity ratio.

Table 6. Diagnostic Performance of Qualitative MR Imaging Characteristics for Diagnosis of Focal Nodular Hyperplasia (FNH) and Hepatocellular Adenoma (HCA).

Characteristic	Sensitivity (%)	Specificity (%)	Accuracy (%)	PPV (%)	NPV (%)	DOR
Qualitative*						
Central scar	—	—	72.9 (63.5; 82.4)	—	—	—
Capsule†	5.3 (0; 11.6)	—	73.8 (64.5; 83.0)	—	72.9 (63.5; 82.4)	—
Fat content	27.5 (9.9; 45.1)	95.3 (90.1; 100.0)	77.1 (68.2; 85.9)	70.0 (41.6; 98.4)	77.6 (68.3; 87.0)	7.05 (1.44; 34.4)
Lobulations	—	—	72.9 (63.5; 82.4)	—	—	—
T1-weighted signal	31.8 (13.3; 50.2)	93.6 (88.0; 99.2)	76.9 (68.2; 85.7)	62.0 (35.6; 88.3)	78.7 (69.4; 87.9)	6.57 (1.80; 24.0)
Portal venous phase	38.9 (20.0; 57.8)	99.0 (96.9; 100.0)	82.2 (74.3; 90.2)	93.8 (81.7; 100.0)	80.3 (71.3; 89.2)	56.9 (6.65; 486.58)
Transitional phase	72.5 (55.1; 89.9)	91.9 (85.6; 98.3)	86.3 (79.3; 93.3)	76.6 (59.8; 93.4)	89.1 (81.4; 96.7)	37.4 (10.51; 133.08)
Hepatobiliary phase	91.9 (82.8; 101.1)	90.1 (82.9; 97.3)	90.1 (84.2; 96.1)	75.9 (60.0; 91.8)	96.6 (92.8; 100.0)	127.1 (28.70; 563.1)
Hepatobiliary enhancement pattern	—	—	72.9 (63.5; 82.4)	—	—	—
Quantitative (cut-offs based on Youden's index)						
CER arterial Cut-off = 106.2	64.4 (47.1; 81.7)	78.0 (68.1; 88.0)	74.1 (65.2; 82.9)	51.6 (34.0; 69.2)	83.0 (73.4; 92.6)	6.67 (2.62; 16.97)
CER portal Cut-off = 110.6	62.0 (44.0; 80.1)	78.0 (68.2; 87.7)	73.4 (64.7; 82.2)	48.4 (30.8; 66.0)	82.9 (73.5; 92.2)	7.76 (2.79; 21.6)

CER transitional Cut-off = 111.5	69.5 (51.4; 87.5)	81.3 (72.3; 90.3)	78.3 (70.1; 86.5)	53.6 (35.8; 71.5)	87.1 (78.8; 95.5)	14.30 (4.76; 42.95)
CER hepatobiliary Cut-off 64.85	75.3 (58.9; 91.8)	76.1 (66.0; 86.1)	75.6 (67.0; 84.3)	50.0 (33.2; 66.8)	88.5 (80.4; 96.6)	13.12 (4.36; 39.50)
LLC arterial Cut-off = 0.596	58.8 (40.4; 77.2)	80.3 (71.3; 89.2)	75.2 (66.9; 83.6)	53.1 (35.8; 70.4)	84.6 (75.8; 93.4)	3.37 (1.30; 8.75)
LLC portal Cut-off = 0.235	89.9 (79.0; 100.0)	17.6 (9.9; 25.4)	38.4 (28.9; 48.0)	28.9 (18.8; 39.1)	84.2 (67.8; 100.0)	1.61 (0.45; 5.8)
LLC transitional Cut-off = -0.07	64.8 (46.7; 83.0)	84.7 (77.2; 92.2)	79.3 (71.5; 87.0)	55.6 (37.5; 73.6)	84.8 (76.2; 93.5)	9.22 (3.2; 26.6)
LLC hepatobiliary Cut-off = -0.2	86.1 (73.0; 99.2)	73.8 (64.3; 83.4)	77.3 (69.4; 85.2)	48.8 (33.5; 64.1)	92.7 (85.8; 99.6)	21.89 (6.3; 76.2)
SIR arterial Cut-off = 1.367	50.4 (31.8; 69.0)	87.8 (80.1; 95.5)	78.7 (70.5; 86.9)	62.5 (43.1; 81.9)	82.4 (73.3; 91.4)	4.33 (1.51; 12.4)
SIR hepatobiliary Cut-off = 0.816	76.0 (60.2; 91.7)	89.6 (83.0; 96.1)	85.6 (79.0; 92.3)	69.9 (53.1; 86.7)	89.1 (81.5; 96.7)	28.71 (9.5; 87.2)
RSER portal Cut-off = 1.056	75.4 (60.3; 90.5)	83.3 (74.8; 91.8)	81.4 (74.0; 88.9)	60.6 (43.9; 77.3)	87.1 (78.8; 95.4)	8.98 (2.98; 27.08)
RSER transitional Cut-off = 0.947	79.1 (65.9; 92.2)	89.4 (82.7; 96.1)	86.4 (80.1; 92.6)	70.3 (53.6; 86.9)	89.2 (81.6; 96.8)	32.49 (11.4; 92.2)
RSER hepatobiliary Cut-off = 0.723	92.6 (84.3; 100.0)	89.4 (82.8; 96.1)	90.2 (84.9; 95.6)	73.0 (57.5; 88.5)	96.5 (92.6; 100)	114.67 (28.22; 465.9)

Note.—* From the nine qualitative imaging features, estimates of diagnostic performance could only be computed for five imaging features included in the CART model. The classification accuracy of four imaging features (central scar, capsule, lobulations, and hepatobiliary enhancement pattern) was insufficient to be included in the proposed CART model. † Specificity, PPV and DOR could not be computed for capsule because there were only 2 out of 140 lesions with a capsule. *CER* = contrast enhacement ratio. *DOR* = diagnostic odds ratio. *LLC* = liver-lesion contrast. *NPV* = negative predictive value. *PPV* = positive predictive value. *RSER* = relative signal enhancement ratio. *SIR* = signal intensity ratio.

FIGURES

Figure 1. Flowchart of patient selection and diagnostic reference.

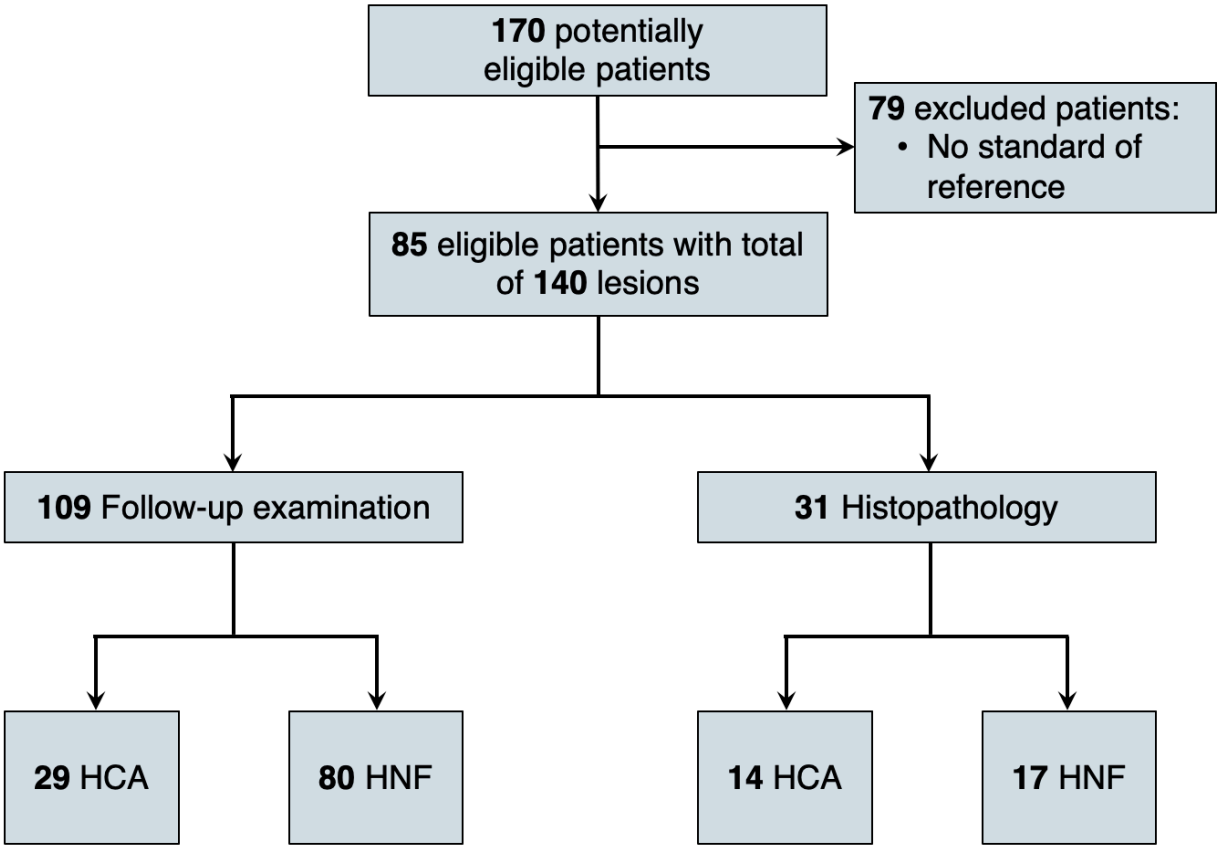

Figure 2. MR images of a biopsy-proven focal nodular hyperplasia in a 47-year-old woman with a 13-mm mass in segment VI of a healthy liver. Top: the mass is isointense to the background liver in T2-weighted sequences without and with fat saturation (arrows), slightly hypointense in T1-weighted in-phase and without signal drop on out-of-phase (arrowheads). Bottom: in dynamic gadoxetate disodium-enhanced phases, the mass presents arterial phase hyperenhancement persistent in portal venous and 5-minute transitional phase with hyperintense signal on the 20-minute hepatobiliary phase.

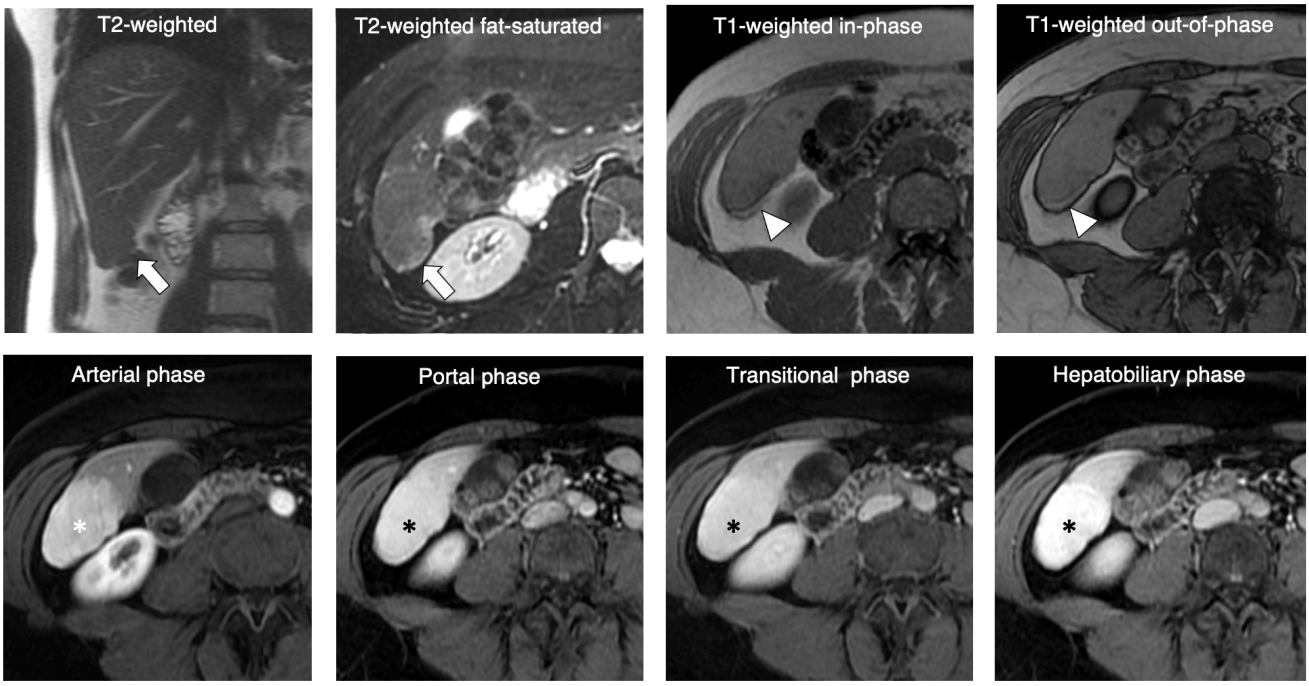

Figure 3. MR images of a pathology proven telangiectatic/inflammatory adenoma in a 30-year-old woman with a 12-mm mass in segment IVa of a healthy liver. Top: the mass is hyperintense signal and heterogenous appearance on T2-weighted sequences without and with fat saturation (arrows), slightly hyperintense in T1 weighted in-phase, without signal drop on out-of-phase sequence (arrowheads). Bottom: in dynamic gadoxetate disodium-enhanced phases, the mass presents arterial phase hyperenhancement, mild hyperenhancement in portal venous phase, hypointense signal in the 5-minute transitional phase and in the 20-minute hepatobiliary phase.

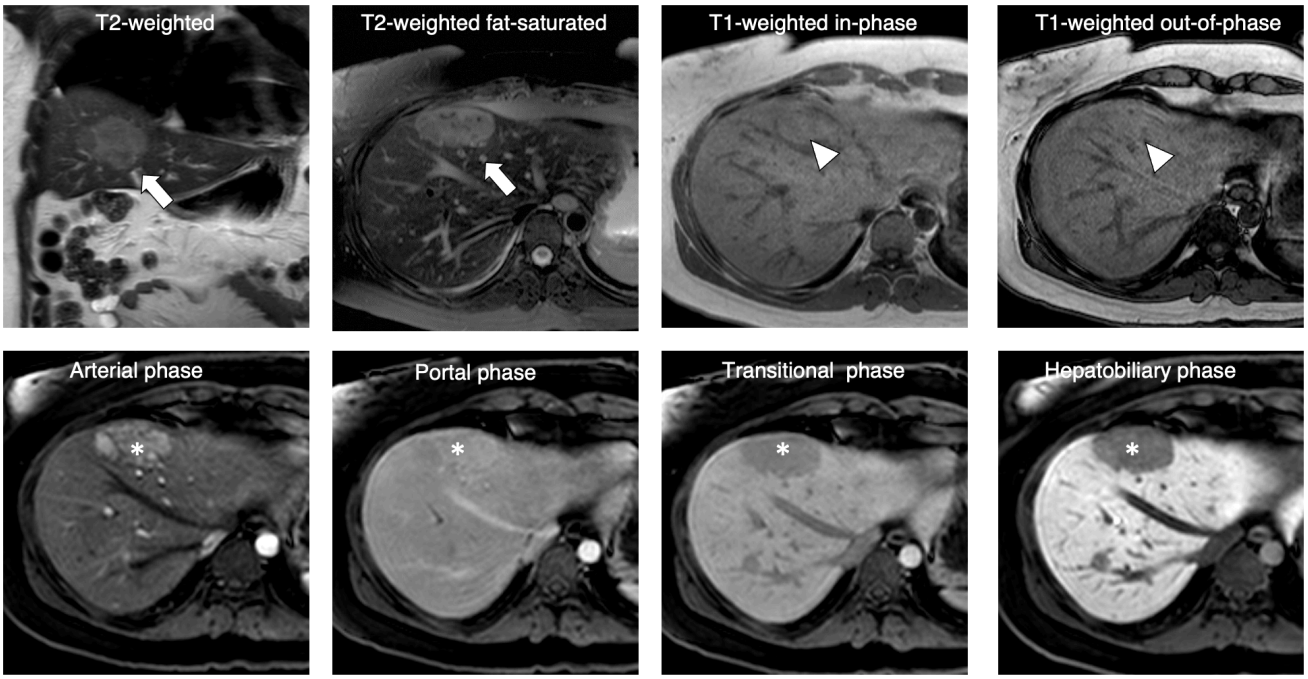

Figure 4. Classification and regression tree (CART) output. The proposed CART is based on five imaging characteristics among the nine enhancement characteristics, morphological features and signal characteristics included in qualitative analysis.